Technical Note

MR Properties of Brown and White Adipose Tissues

Gavin Hamilton, PhD,[1] Daniel L. Smith,Jr, PhD,[2] Mark Bydder, PhD,[1] Krishna S. Nayak, PhD,[3] and Houchun H. Hu, PhD[3]*

Purpose: To explore the MR signatures of brown adipose tissue (BAT) compared with white adipose tissue (WAT) using single-voxel MR spectroscopy.

Materials and Methods: ^{1}H MR STEAM spectra were acquired from a 3 Tesla clinical whole body scanner from seven excised murine adipose tissue samples of BAT (n = 4) and WAT (n = 3). Spectra were acquired at multiple echo times (TEs) and inversion times (TIs) to measure the T1, T2, and T2-corrected peak areas. A theoretical triglyceride model characterized the fat in terms of number of double bonds (ndb) and number of methylene-interrupted double bonds (nmidb).

Results: Negligible differences between WAT and BAT were seen in the T1 and T2 of fat and the T2 of water. However, the water fraction in BAT was higher (48.5%) compared with WAT (7.1%) and the T1 of water was lower in BAT (618 ms) compared with WAT (1053 ms). The fat spectrum also differed, indicating lower levels of unsaturated triglycerides in BAT (ndb = 2.7, nmidb = 0.7) compared with WAT (ndb = 3.3, nmidb = 1.0).

Conclusion: We have demonstrated that there are several key MR-based signatures of BAT and WAT that may allow differentiation on MR imaging.

Key Words: proton MR spectroscopy; triglyceride; brown and white adipose tissue; relaxation properties; fat fraction
J. Magn. Reson. Imaging 2011;34:468–473.
© 2011 Wiley-Liss, Inc.

BROWN ADIPOSE TISSUE (BAT) is a topic of great interest in obesity and metabolism research and recent reports (1–5) continue to investigate its extent and physiological function, particularly in humans (6–8). Whereas white adipose tissue (WAT) is characterized by adipocytes containing a large, unilocular, intracellular lipid droplet and limited cytoplasm, BAT contains adipocytes with multiple, smaller, intracellular lipid droplets and an abundance of iron-rich mitochondria (9). BAT is involved in energy expenditure and thermogenesis. It is more vascularized than WAT, densely innervated by the sympathetic nervous system, and exhibits significant metabolic activity upon stimulation (9).

While there have been many articles reporting the incidental identification of BAT with positron emission and computed tomography (PET/CT) (6,10–12), prospective, investigational/physiological studies of BAT in humans remain limited. This may be due to the fact that PET/CT is recommended for clinically warranted reasons in patients and is not broadly applicable in healthy subjects due to costly radiotracer usage and radiation exposure, although a few prospective studies with healthy human subjects have been reported (6–8). Another reason is that, while the anatomical distribution of BAT depots in rodents is known and the interscapular BAT depot is well-delineated from other surrounding tissues, similar information describing the absolute amount and anatomical distribution in adult humans is limited.

Several works have successfully imaged and characterized differences in BAT and WAT in animals with MR, in particular using spectroscopy (MRS) and chemical-shift-imaging (CSI) methods (13–15). Due to BAT's histological and physiological characteristics, its fat fraction as measured by MRS and CSI is lower than that of lipid-rich WAT. However, the usage of fat fraction marker alone may not be adequate in identifying human BAT depots in vivo due to partial volume effects from limited spatial resolution and the fact that the tissue exists in very small localized foci (16,17).

The purpose of this study is to explore other potential BAT-specific MR signatures in addition to the fat fraction metric. We hypothesize that additional physical properties such as T1 relaxation time and the degree of lipid saturation can be used in conjunction with fat fraction to differentiate BAT from WAT.

MATERIALS AND METHODS

Animal Samples

Excised tissue samples of interscapular BAT, the largest known BAT depot in rodents, and gonadal WAT

[1]Department of Radiology, University of California, San Diego, San Diego, California, USA.
[2]Department of Nutrition Sciences, University of Alabama at Birmingham, Birmingham, Alabama, USA.
[3]Ming Hsieh Department of Electrical Engineering, University of Southern California, Los Angeles, California, USA.
Contract grant sponsor: National Institutes of Health; Contract grant numbers: R21DK081173, K25DK087931, P30DK56336, P60DK079626, T32DK062710.
*Address reprint requests to: H.H.H., University of Southern California, 3740 McClintock Avenue, Electrical Engineering Building 408, Los Angeles, CA. 90089-2564. E-mail: houchunh@usc.edu
Received September 22, 2010; Accepted March 28, 2011.
DOI 10.1002/jmri.22623
View this article online at wileyonlinelibrary.com.

© 2011 Wiley-Liss, Inc.

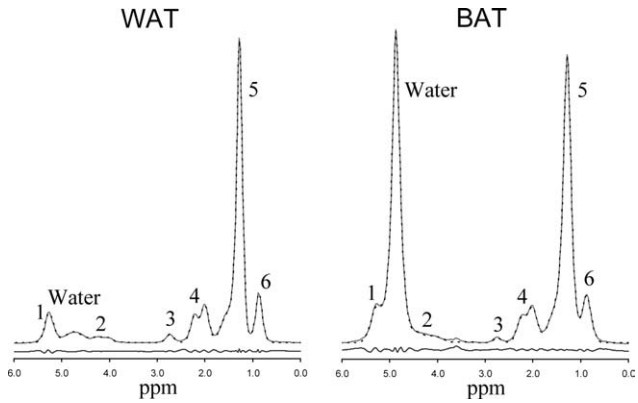

Figure 1. Representative white (left) and brown (right) adipose tissue MR spectrum at 3 Tesla (TR 5000 ms, TE 13 ms). Of the six fat peaks resolvable by spectroscopy at 3 Tesla, two peaks (peak 1 at 5.19–5.29 ppm and peak 2 at 4.2 ppm) are buried under the large water peak in BAT. The MRUI generated fit (dotted line) is also shown along with the residues of the fit.

were obtained from ~20 week old A/J female (The Jackson Laboratory; Bar Harbor, ME) mice carcasses (n = 15; body weight: 22.1 ± 1.2 grams [mean ± SD]). Additional cohorts of B6*129 mixed background mice were also used for interscapular BAT and gonadal WAT tissue collection (n = 7 females: body weight: 20.0 ± 1.4, 6 ± 1 weeks of age; n = 10 females: body weight 19.3 ± 2.3, 6 ± 1 weeks of age; n = 4 males: body weight 34.4 ± 4.5 grams, 14 weeks of age). A/J mice were singly housed and B6*129 mice were group house (n < 5) in standard cages at 22 ± 1°C with a 12:12 light:dark cycle and provided ad libitum access to a standard rodent diet. Tissue samples were acquired postmortem and pooled within each group in a single 1.5-mL microtube at the University of Alabama at Birmingham. During tissue dissection, care was taken to ensure that only the interscapular BAT depot was excised and that very little contribution from the adjacent dorsal WAT layer was included. Likewise for the gonadal WAT depots, unwanted contributions to the sample from surrounding soft tissues were also minimized. The excised adipose tissue was pooled into four BAT and three WAT samples. The pooled BAT samples were pooled within the same strain and sex and relative age. The samples were then immediately shipped by overnight courier service to investigators at the University of California San Diego for MRS evaluation. All animal research was conducted in accordance with the local Institutional Animal Care and Use Guidelines.

Characterization of Fat Spectrum

Each of the resonance peaks present in the fat ^{1}H MR spectrum (Fig. 1) represents a distinct proton moiety (Table 1) (18,19). Spectroscopy can use knowledge of the triglyceride chemical structure to determine the type of triglyceride present. A detailed description of the MRS method used in this work has been published (20). Briefly, the relative area of each of the peaks was found by adding the number of hydrogen nuclei with its associated type of bond in the triglyceride molecule. For example, each of the three fatty acid chains was terminated by a CH_3 giving a total signal of nine signal units for the 0.9 ppm peak. Similarly, as each double bond had two CH groups associated with it, the relative area of the 5.3 ppm peak was given by 2*number of double bonds. Thus we can specify the chemical structure of the triglyceride in terms of three variables: number of –CH = CH – double bonds per molecule (ndb), number of double bonds separated by a single CH_2 (nmidb – number of methylene-interrupted double bonds), and the fatty acid chain length (CL) (20).

MRS Acquisitions

The ^{1}H MR spectra were acquired on a 3 Tesla (GE Signa EXCITE HD, GE Healthcare, Waukesha, WI) human whole body scanner. All scans were carried out at room temperature. Spectra were collected using a 3-cm-diameter birdcage coil. A 4 × 4 × 4 mm voxel was selected and shimmed after conventional imaging. The Stimulated Echo Acquisition Mode (STEAM) sequence was chosen to allow a shorter minimum echo time (TE) (21), minimizing J-coupling effects. Five spectra with 16 signal averages were acquired at progressively longer TEs of 13, 18, 22, 28, and 33 ms. The mixing time (TM) was fixed at a minimum value of 6 ms. The TM and range of TE values were chosen to minimize J-coupling effects (22). A repetition time (TR) of 5000 ms was chosen to avoid T1 weighting. Multi-TE acquisition allowed calculation of T2 and T2-corrected area of the individual spectral peaks (23,24). To measure T1 spectra were collected at minimum TE

Table 1
Peak Assignments and Relative Magnitude of Triglyceride Peak Areas, Following (20)

Peak	Location	Assignment	Relative magnitude	In vivo ppm
1	5.29 ppm	-C**H**=C**H**-	ndb*2	5.3 ppm
	5.19 ppm	-C**H**-O-CO-	1	
Water	4.8 ppm	$\mathbf{H_2}$O	–	4.8 ppm
2	4.2 ppm	-C$\mathbf{H_2}$-O-CO-	4	4.2 ppm
3	2.75 ppm	-CH=CH-C$\mathbf{H_2}$-CH=CH-	nmidb*2	2.75 ppm
4	2.20 ppm	-CO-C$\mathbf{H_2}$-CH$_2$-	6	2.1 ppm
	2.02 ppm	-C$\mathbf{H_2}$-CH=CH-C$\mathbf{H_2}$-	(ndb-nmidb)*4	
5	1.6 ppm	-CO-CH$_2$-C$\mathbf{H_2}$-	6	1.3 ppm
	1.3 ppm	-(C$\mathbf{H_2}$)$_n$-	[(CL-4)*6]-(ndb*8) + (nmidb*2)	
6	0.90 ppm	-(CH$_2$)$_n$-C$\mathbf{H_3}$	9	0.9 ppm

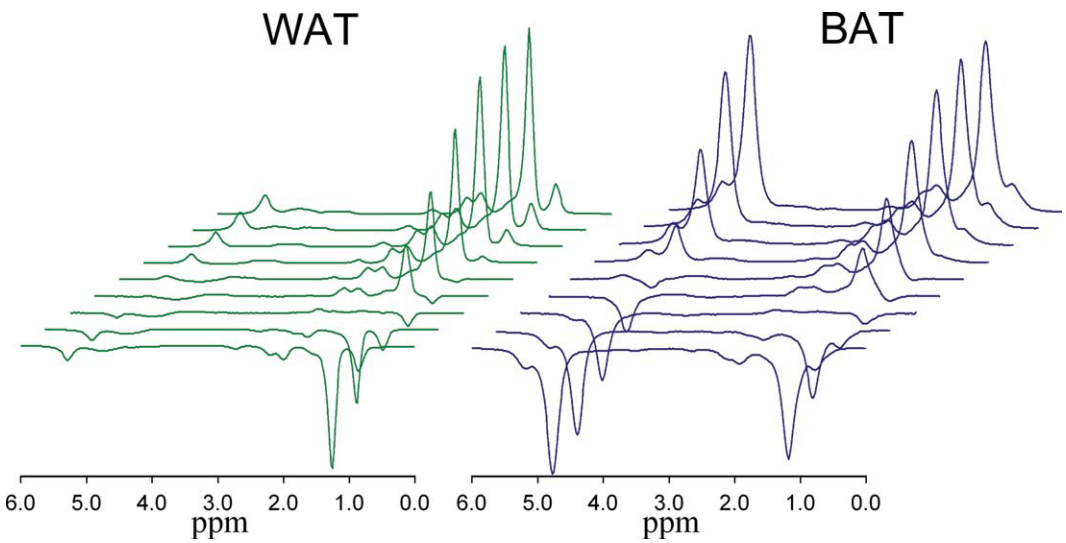

Figure 2. Change in the white (left) and brown (right) adipose tissue MR spectrum (TR 5000 ms, TE 13 ms) with increasing TI (50, 100, 200, 300, 400, 600, 1000, 2000, and 4000 ms). [Color figure can be viewed in the online issue, which is available at wileyonlinelibrary.com.]

of 13 ms and inversion times (TIs) of 50, 100, 200, 300, 400, 600, 1000, 2000, and 4000 ms. There was no water saturation, and spatial saturation bands around the voxel were disabled to ensure a uniform spectral response across the frequency range of interest.

MRS Analyses

The spectra were analyzed using the AMARES algorithm (25), included in the MRUI software package (26). All the fat peaks were modeled by multiple Gaussian resonances. The T1, T2, and the T2-corrected peak areas were calculated by nonlinear least-square fitting. To characterize the triglyceride composition of WAT, ndb and nmidb were calculated by nonlinear least-square fitting of the measured areas of peaks 1, 3, 4, 5, and 6 to the theoretical model (Table 1). For BAT, only peaks 3–6 were used, as peaks 1 and 2 overlapped the water peak and were unable to be clearly distinguished.

J-coupling causes the behavior of fat peaks to be no longer strictly described by T2 decay. The effect of J-coupling increases as TE increases, and the short TE range used in this study minimizes its effect (27). However, fat peak 2 is a strongly coupled AB spin system, and is more strongly coupled than the other fat peaks (19). J-coupling is evident in this peak even at the shortest TE, so peak 2 was not used in our analysis.

RESULTS

Representative spectra from brown and white adipose tissue are shown in Figure 1. While the water peak is the dominant peak in the BAT spectrum, several of the fat peaks are larger than the water peak in the WAT spectrum, due to the low water fraction in WAT. The peaks are slightly broadened in BAT due to either higher iron content or differences in magnetic field homogeneity inside the sample. Figure 2 shows the

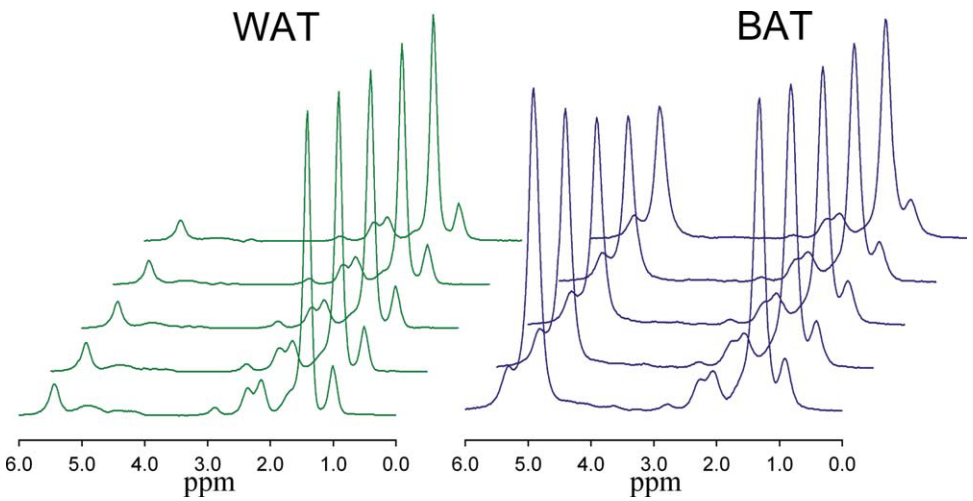

Figure 3. Change in the white (left) and brown (right) adipose tissue MR spectrum (TR 5000 ms) with increasing TE (13, 18, 23, 28, and 33 ms). [Color figure can be viewed in the online issue, which is available at wileyonlinelibrary.com.]

Table 2
Mean (and Range) of T1, T2, and T2-Corrected Peak Areas for White Adipose Tissue*

Peak	In vivo ppm	Assignment	T1 (ms)	T2 (ms)	Measured signal	Calculated signal
1	5.3 ppm	-C**H**=C**H**- -C**H**-O-CO-	421 (406–436)	44.1 (42.6–45.6)	0.127 (0.109–0.145)	0.122 [7.6 %]
Water	4.7 ppm	$\mathbf{H_2}$O	1053 (1005–1101)	21.7 (17.3–26)	0.124 (0.119–0.148)	–
2	4.2 ppm	-C$\mathbf{H_2}$-O-CO-	154 (145–163)	–	–	0.064 [4.0 %]
3	2.75 ppm	-CH=CH-C$\mathbf{H_2}$-CH=CH-	284 (274–294)	46.2 (44.5–47.9)	0.027 (0.023–0.033)	0.033 [2.0 %]
4	2.1 ppm	-CO-C$\mathbf{H_2}$-CH$_2$- -C$\mathbf{H_2}$-CH=CH-C$\mathbf{H_2}$-	202 (194–210) 249 (238–259)	51.9 (51.8–52.1)	0.238 (0.237–0.238)	0.241 [15.0 %]
5	1.3 ppm	-CO-CH$_2$-C$\mathbf{H_2}$- -(C$\mathbf{H_2}$)$_n$-	240 (214–264) 280 (268–292)	54.7 (42.8–61.4)	1.000	1.000 [62.4 %]
6	0.9 ppm	-(CH$_2$)$_n$-C$\mathbf{H_3}$	543 (434–616)	80.1 (50.7–110.2)	0.147 (0.140–0.158)	0.144 [9.0 %]

*The final column gives predicted areas for ndb = 3.3 and nmidb = 1.0 [% total fat].

typical signal variation with TI measured in single WAT and BAT samples, and Figure 3 shows signal variation with TE in the same tissues.

Table 2 shows the mean and range of T1, T2, and T2-corrected peak areas of WAT. Using the mean T2-corrected areas of peaks 1, 3, 4, 5, and 6 in the fat model (described in the Methods section) gives ndb = 3.3 and nmidb = 1.0. The predicted fat peak areas given by these values are also shown in Table 2. This indicates that the mean water signal comprises 7.1% of the total signal.

Table 3 shows the mean and range of T1, T2 and T2-corrected peak areas of BAT. The T2 of peaks 1 and 2 could not be determined due to the large water peak, although the T1 of peak 1 could be determined. Using the mean T2-corrected areas of visible fat peaks (peaks 3, 4, 5 and 6) gives ndb = 2.7 and nmidb = 0.7. The expected peak areas given by these values are also shown in Table 3 and indicate that 10.3% of the fat signal underlies the water peak in BAT. Allowing for this correction, the mean water signal comprises 48.5% of the total signal.

Summarizing the results for WAT and BAT in Tables 2 and 3, no differences were seen in the T2 values of any of the peaks. Also, the T1 of the fat peaks were similar. However, higher levels of water were observed in BAT compared with WAT, as reported previously, and the T1 of water in WAT was higher as demonstrated in Figure 4. The triglyceride in BAT also was more saturated than in WAT.

DISCUSSION

In this ex vivo study, the MR properties of murine brown and white adipose tissue were assessed by MRS using a whole-body 3 Tesla clinical scanner. The purpose was to explore potential BAT- and WAT-specific MR signatures in addition to the known fat fraction differences. The results have demonstrated several key physical properties that are different between BAT and WAT: fat fraction, T1 relaxation rate of the water component, and the degree of lipid saturation.

When we compared BAT and WAT using MRS, the most obvious differences were seen in the water peak behavior. In WAT, water is a small component of the total signal. In contrast, the water signal is of similar magnitude to the fat signal in BAT. There were also differences in water T1 with the value measured in WAT being almost double that of the water T1 in BAT, which agrees with previous observations (28).

The T1 and T2 of the multiple fat peaks were similar for both BAT and WAT. However, the peak areas were found to be different due to the different types of triglycerides present. Our results also suggest that WAT has higher ndb and nmidb values than BAT, indicating that WAT has a greater proportion of unsaturated triglycerides. The degree of saturation of WAT and BAT has been measured previously at 500 MHz (29). In WAT, the ndb and nmidb values reported were 3.45 and 1.29, respectively, which are in close agreement with values measured in this study. In BAT, a range

Table 3
Mean (and Range) of T1, T2, and T2-Corrected Peak Areas for Brown Adipose Tissue*

Peak	In vivo ppm	Assignment	T1 (ms)	T2 (ms)	Measured signal	Calculated signal
1	5.3 ppm	-C**H**=C**H**- -C**H**-O-CO-	–	–	–	0.098 [6.4 %]
Water	4.7 ppm	$\mathbf{H_2}$O	618 (588–669)	21.1 (18.1–22.9)	1.605 (0.901–1.865)	–
2	4.2 ppm	-C$\mathbf{H_2}$-O-CO-	–	–	–	0.060 [3.9 %]
3	2.75 ppm	-CH=CH-C$\mathbf{H_2}$-CH=CH-	219 (154–294)	41.4 (32.3–48.7)	0.016 (0.012–0.020)	0.019 [1.2 %]
4	2.1 ppm	-CO-C$\mathbf{H_2}$-CH$_2$- -C$\mathbf{H_2}$-CH=CH-C$\mathbf{H_2}$-	189 (156–216) 247 (235–265)	55.3 (47.8–59.6)	0.216 (0.213–0.219)	0.218 [14.2 %]
5	1.3 ppm	-CO-CH$_2$-C$\mathbf{H_2}$- -(C$\mathbf{H_2}$)$_n$-	239 (227–265) 278 (271–292)	51.8 (46.7–55.1)	1.000	1.000 [65.3 %]
6	0.9 ppm	-(CH$_2$)$_n$-C$\mathbf{H_3}$	567 (544–591)	61.5 (50.9–71.3)	0.149 (0.138–0.164)	0.136 [8.9 %]

*The final column gives predicted areas for ndb = 2.7 and nmidb = 0.6 [% total fat].

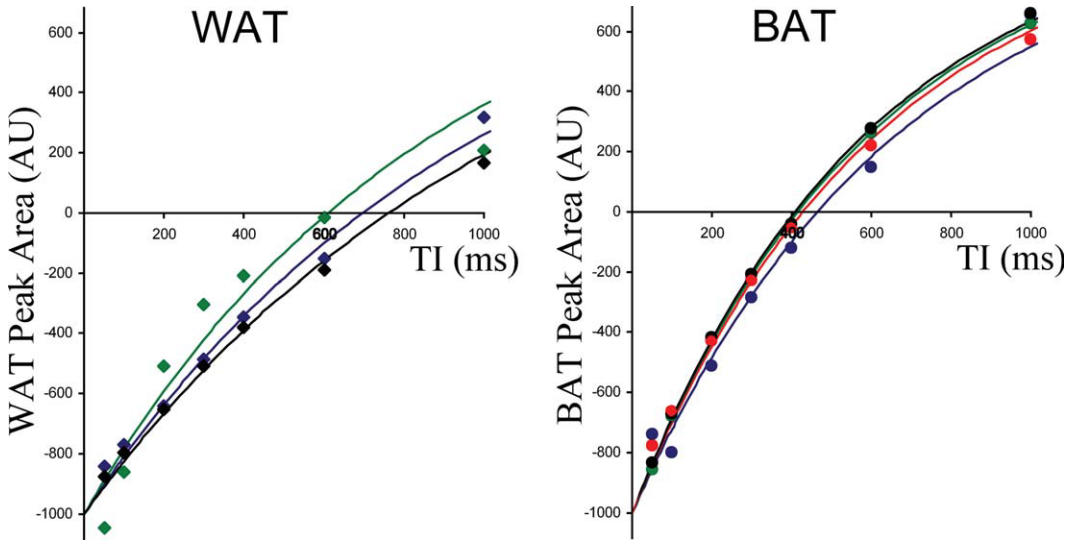

Figure 4. The inversion recovery behavior measured in the water peak in each of the samples of white (left) and brown (right) adipose tissue. The fully recovered water signal is normalized to 1000 AU to allow comparison of the different tissues.

of values was reported (ndb 2.49–3.63 and nmidb 0.96–1.81) with the degree of saturation depending on age. The range of BAT nmidb was higher than the value found in this study. It should be noted that ~3-month-old rats were used for adipose tissue samples. We speculate that, although they were housed under similar conditions to the mice used in this study, their larger body mass and slightly older age compared with the mice used here could both influence the activity of BAT, and potentially alter the tissue saturation characteristics.

The differences observed by MRS provide a noninvasive approach for differentiating BAT from WAT. It should be noted that differences in fat fraction, T1 relaxation, and lipid saturation are all based on endogenous biochemical and histological characteristics, in contrast to PET/CT approaches that require metabolically active BAT to uptake exogenous radiotracer for identification. Consequently, these differences should be observable in BAT regardless of the tissue's activation state. One drawback of in vivo spectroscopy is its limited spatial resolution. MR imaging-based methods can provide sufficient spatial resolution, but require information about the relaxation properties, chemical shifts and/or relative spectral peak areas to optimize sensitivity for detection.

One of the primary functions of BAT is to produce heat in nonshivering thermogenesis. When the tissue is stimulated, local temperature in the vicinity of BAT can rise. The chemical shift position of water and fat is dependent on temperature (30). Thus, the ppm difference in chemical shift between water and methylene peaks can potentially reflect active and inactive BAT. We were not able to quantify this effect in the present ex vivo study. The feasibility and sensitivity of a temperature-based MRS marker for BAT requires further investigation.

The T1 and T2 values measured here may not agree with the values found in vivo due to body temperature. Although T1, T2, and even the chemical shift of the spectral peaks are temperature dependent, WAT and BAT should be affected in a similar manner, and hence similar relative differences would be expected in vivo. Past literature has also shown that brown adipocytes can contain varying sizes of lipid droplets, depending on the tissue's level of stimulation and activity state amongst subjects (16,17). Furthermore, recent findings have also suggested that certain BAT cells can differentiate from WAT progenitors and exhibit an intermediate phenotype that satisfies both classical definitions of BAT and WAT (31–33). In contrast, the cytology of white adipocytes has been more consistent across subjects and studies.

In the present study, tissue samples were pooled to obtain sufficient volume to allow MRS data acquisition using our clinical system. This may have masked differences in individual samples from different animals and is a recognized limitation of the work. The requirement for a sufficient volume will limit spatial resolution, possibly limiting its ability to detect BAT. However, the BAT-specific information generated here can be used in MR imaging techniques that incorporate the properties of the multi-peak spectral structure of adipose tissue, which may eventually lead to more sophisticated MRI-based BAT detection methods.

In conclusion, this article has demonstrated several differences in the MR signatures of BAT and WAT that can provide a basis for optimizing imaging techniques for differentiating the two tissues.

ACKNOWLEDGMENTS

K.S.N., H.H.H., and D.L.S. were funded by the National Institutes of Health.

REFERENCES

1. Himms-Hagen J. Obesity may be due to a malfunctioning of brown fat. Can Med Assoc J 1979;121:1361–1364.

2. Himms-Hagen J. Thermogenesis in brown adipose tissue as an energy buffer. Implications for obesity. N Engl J Med 1984;311: 1549–1558.
3. Cannon B, Nedergaard J. Brown adipose tissue: function and physiological significance. Physiol Rev 2004;84:277–359.
4. Nedergaard J, Cannon B. The changed metabolic world with human brown adipose tissue: therapeutic visions. Cell Metab 2010;11:268–272.
5. Enerback S. Human brown adipose tissue. Cell Metab 2010;11: 248–252.
6. van Marken Lichtenbelt WD, Vanhommerig JW, Smulders NM, et al. Cold-activated brown adipose tissue in healthy men. N Engl J Med 2009;360:1500–1508.
7. Wijers SL, Saris WH, van Marken Lichtenbelt WD. Cold-induced adaptive thermogenesis in lean and obese. Obesity 2010;18: 1092–1099.
8. Yoneshiro T, Aita S, Matsushita M, et al. Brown adipose tissue, whole-body energy expenditure, and thermogenesis in healthy adult men. Obesity 2011;19:13–16.
9. Cinti S. The role of brown adipose tissue in human obesity. Nutr Metab Cardiovasc Dis 2006;16:569–574.
10. Lee P, Ho KK, Fulham MJ. The importance of brown adipose tissue. N Engl J Med 2009;361:418; author reply 419–420.
11. Cypess AM, Lehman S, Williams G, et al. Identification and importance of brown adipose tissue in adult humans. N Engl J Med 2009;360:1509–1517.
12. Pfannenberg C, Werner MK, Ripkens S, et al. Impact of age on the relationships of brown adipose tissue with sex and adiposity in humans. Diabetes 2010;59:1789–1793.
13. Lunati E, Marzola P, Nicolato E, Fedrigo M, Villa M, Sbarbati A. In vivo quantitative lipidic map of brown adipose tissue by chemical shift imaging at 4.7 Tesla. J Lipid Res 1999;40:1395–1400.
14. Hu HH, Smith DL Jr, Nayak KS, Goran MI, Nagy TR. Identification of brown adipose tissue in mice with fat-water IDEAL-MRI. J Magn Reson Imaging 2010;31:1195–1202.
15. Branca RT, Warren WS. In vivo brown adipose tissue detection and characterization using water-lipid intermolecular zero-quantum coherences. Magn Reson Med 2011;65:313–319.
16. Heaton JM. The distribution of brown adipose tissue in the human. J Anat 1972;112:35–39.
17. Tanuma Y, Tamamoto M, Ito T, Yokochi C. The occurrence of brown adipose tissue in perirenal fat in Japanese. Arch Histol Jpn 1975;38:43–70.
18. Fauhl C, Reniero F, Guillou C. 1H NMR as a tool for the analysis of mixtures of virgin olive oil with oils of different botanical origin. Magn Reson Chem 2000;38:436–443.
19. Oostendorp M, Engelke UF, Willemsen MA, Wevers RA. Diagnosing inborn errors of lipid metabolism with proton nuclear magnetic resonance spectroscopy. Clin Chem 2006;52:1395–1405.
20. Hamilton G, Yokoo T, Bydder M, et al. In vivo characterization of the liver fat 1H magnetic resonance spectrum. NMR Biomed 2010 [Epub ahead of print] doi:10.1002/nbm.1622.
21. Keevil SF. Spatial localization in nuclear magnetic resonance spectroscopy. Phys Med Biol 2006;51:R579–R636.
22. De Graff RA, Rothman DL. In vivo detection and quantification of scalar coupled 1H NMR resonances. Concept Magn Reson 2001; 13:32–76.
23. Ren J, Dimitrov I, Sherry AD, Malloy CR. Composition of adipose tissue and marrow fat in humans by 1H NMR at 7 Tesla. J Lipid Res 2008;49:2055–2062.
24. Querleux B, Cornillon C, Jolivet O, Bittoun J. Anatomy and physiology of subcutaneous adipose tissue by in vivo magnetic resonance imaging and spectroscopy: relationships with sex and presence of cellulite. Skin Res Technol 2002;8:118–124.
25. Vanhamme L, van den Boogaart A, Van Huffel S. Improved method for accurate and efficient quantification of MRS data with use of prior knowledge. J Magn Reson 1997;129:35–43.
26. Naressi A, Couturier C, Devos JM, et al. Java-based graphical user interface for the MRUI quantitation package. MAGMA 2001; 12:141–152.
27. Hamilton G, Middleton MS, Bydder M, et al. The effect of PRESS and STEAM sequences on magnetic resonance spectroscopic liver fat quantification. J Magn Reson Imaging 2009;20: 145–152.
28. Hu HH, Nayak KS. Change in the proton T1 of fat and water in mixture. Magn Reson Med 2009;63:494–501.
29. Zancanaro C, Nano R, Marchioro C, Sbarbati A, Boicelli A, Osculati F. Magnetic resonance spectroscopy investigations of brown adipose tissue and isolated brown adipocytes. J Lipid Res 1994; 35:2191–2199.
30. Soher BJ, Wyatt C, Reeder SB, MacFall JR. Noninvasive temperature mapping with MRI using chemical shift water-fat separation. Magn Reson Med 2010;63:1238–1246.
31. Petrovic N, Shabalina IG, Timmons JA, Cannon B, Nedergaard J. Thermogenically competent nonadrenergic recruitment in brown preadipocytes by a PPARgamma agonist. Am J Physiol Endocrinol Metab 2008;295:E287–E296.
32. Petrovic N, Walden TB, Shabalina IG, Timmons JA, Cannon B, Nedergaard J. Chronic peroxisome proliferator-activated receptor gamma (PPARgamma) activation of epididymally derived white adipocyte cultures reveals a population of thermogenically competent, UCP1-containing adipocytes molecularly distinct from classic brown adipocytes. J Biol Chem 2010;285:7153–7164.
33. Barbatelli G, Murano I, Madsen L, et al. The emergence of cold-induced brown adipocytes in mouse white fat depots is determined predominantly by white to brown adipocyte transdifferentiation. Am J Physiol Endocrinol Metab 2000;298:E1244–E1253.